Using the Spatial Light Modulator for Adaptive Optics in Fluorescence Microscopy

Utrecht University

Author
Peter Elroy

Supervisors
Prf. Dr. H.C. Gerritsen
Dr. Gerhard Blab

November 7, 2014

Abstract

To improve the quality of Stimulated Emission Depletion microscopy for the study of the physiology of Epidermal Growth Factor, challenges and possibilities of depletion beam pattern formation are assessed using a Spatial Light Modulator. The fluorescence depletion spot is analyzed without sample interaction, using high-resolution imaging of the spot shape under a high diffraction limit. Software is developed to gain full control over the depletion spots and analytical tools are written to determine correction schemes for them. Due to the benefit of parallel con-focal measurements, the quality analysis extends to the generation of multiple depletion beams using a single SLM.

Contents

1 Introduction

The field of microscopy underwent great advancement when fluorescence microscopy was established. This technique allowed for the detection and tracking of otherwise unobservable bodies by associating them with fluorophores that will fluoresce through interaction with a focused laser 'activation' spot. However, the resolution was limited by the smallest size of the focal spot; the Abbe diffraction limit.

The applications of fluorescence microscopy underwent a significant expansion in 1994 through the introduction of Stimulated Emission Depletion (STED) microscopy [4], allowing super-resolution microscopy; light microscopy with an image resolution beyond the diffraction limit. It opened up new scales of phenomena to light microscopy observation, most notably in the field of biology, where many processes within cell components can take on dimensions below 230 nm.

A particular point of interest in biology are Bio-molecular interactions, which are an important part of cell dynamics. Typically, they are studied through the use of Frster Resonance Energy Transfer (FRET) Microscopy. However, a significant limitation of this method is its short detection radius, which is approximately 10 nm. Any Bio-molecular interactions that exceeds this dimension, such as those of oligomers, goes undetected when using FRET. While they are too large to be detected by FRET, they are still below that 230 nm dimension which normal light microscopy is approximately limited to. This puts them right inside a gap of accessible scales. To bridge this gap, STED microscopy can be used. We want to be able to study the Epidermal Growth Factor (and also the Epidermal Growth Factor Receptor) in endocytosis, which plays a vital role in cancer.

STED takes a group of fluorophores activated using a focal spot, and depletes the outer ring using a depletion spot. In the center of this laser spot, a small region of zero intensity ensures that a small cluster of fluorophores is left active. This dark area can achieve significantly smaller dimensions than the activation spot, allowing for smaller, more localized areas of fluorescence to be measured.

The shape of the depletion spot strongly influences the effectiveness of STED microscopy. This shape is determined by the method used for the generation of the depletion spot, but can also be perturbed by aberrations contracted either within the microscope or when interacting with the sample. These aberrations can change drastically as the sample shifts and the microscope drifts away from its optimization, creating a demand for adaptive optics; a feedback system in which the optics dynamically adapt to aberrations as they occur. While conventional optics is able to provide such a system [7], the complexity of this approach increases dramatically as aberrations become stronger and larger in number.

A more unified approach, where all optical manipulations are performed on one surface and are controlled through a single digital interface, is offered by the use of a Spatial Light Modulator (SLM) [2]. The SLM provides a diffracting grid, in which each grid square can modulate the phase of the incident beam section. The resulting phase mask will induce an interference pattern that can be designed to create desired intensity patterns without diminishing the overall intensity. This gives great freedom over the shape of the depletion spot, and allows for great flexibility when adjusting the beam shape to compensate for perturbing factors.

The central benefits of the SLM stem from two properties; it modulates phase instead of intensity and the controls are digital instead of analogue, making it easy to control through software. However, these features also impose drawbacks. To produce an appropriate phase mask for an intended intensity pattern of the depletion spot, some conversion equation or algorithm is required, and the discrete steps to which it is restricted inherently limit the nuance of the phase mask.

2 STED Microscopy

In this section, STED microscopy is introduced in more detail, the constructed STED set-up is described and the trail experiments performed with it are treated.

2.1 Introduction

In order to create a set-up for high-resolution microscopy of biological samples, a STED microscope is being built. A pulsed laser is split into two separate beams, of which one is used as the activation beam which is brought to a wavelength of 642 nm, and the other as the depletion beam which is brought to a wavelength of 780 nm. The required donut-like shape for the depletion beam is generated using a liquid crystal SLM and the reflected beam is then reflected at a 90 degree angle after which it can be sent towards the microscope aperture. The activation beam is also sent towards the aperture after having passed through a pinhole, so that a clean Airy disk pattern is created.

2.2 Fluorophore

Fluorophores are chemical compounds that can emit light when light is shone upon it. They are activated by bringing the fluorophore from its ground state to an emitting state. It is a material that is very visible for light detectors, which is why it is frequently used in microscopy. To activate a fluorophore, the energy difference between the two states must be matched by the photon energy of the illuminating beam in order to activate the fluorophore.

The depletion of the fluorescent state performed by STED works in a similar way. The fluorescent state of the fluorophore is depleted into a higher energy state by providing light of which the energy is tuned to the energy difference of the two states. This energy is generally not equal to the activation energy, therefore two separately controlled light wavelengths are required to perform STED. The exact wavelengths depend on the used fluorophore.

The fluorophore that we have used is one that is frequently applied to fluorescence microscopy; ATTO 647N. The bandwidth in which it fluoresces, as can be seen from Figure 1, lies mostly in the region of red light. In the same figure it is also shown that the wavelength at which ATTO 647N absorbs light overlaps with that of its fluorescence. Care must be taken in choosing a wavelength that will activate the fluorophore and will not be confused with fluorescence when measuring the sample's light signal. Our usage of a 742 nm activation and 780 nm depletion beam meets this requirement.

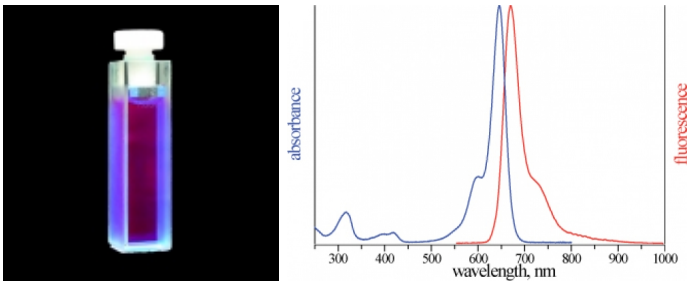

(a) Vial containing ATTO 647N

(b) Absorption and emission

Figure 1: ATTO 647N

2.3 Depletion Spot

Emitting fluorophores are easily detected, but when a large spot of fluorophores is activated as a whole, it is not possible to distinguish a pattern within that spot. The fluorescence is measured as one intensity value. In order to detect structure in the fluorophores, several spots must be measured separately and each will be treated as a pixel within a total image. Reducing the spot size of the image increases the resolution. This has been done in regular fluorescence microscopy to the point where the Abbe diffraction limit is reached.

The Abbe limit states that light, when traveling with wavelength λ and converging to a spot with an angle θ, will come to a minimal beam waist with radius

$$d = \frac{\lambda}{2n \sin \theta} = \frac{\lambda}{2NA} \tag{1}$$

where NA is the numerical aperture.

Having a trough in the intensity pattern surrounded by a crest is the defining characteristic of the depletion spot, along with this trough being smaller in size than the activation beam used to initiate fluorescence. The most simplistic way of achieving such a trough is by using a ring pattern in the focal plane, also called a donut. Using such a simple pattern allows the spot to be stable and easy to generate.

The most simple donut type beam is found by solving the par-axial wave equations for our minimum requirement, which is that the beam is cylindrically symmetric. The common family of solutions to this requirement are the Laguerre-Gaussian modes, seen in Figure 2. Here the indexing refers to the common LG mode notation LG_p^l. It shows that for increasing values of p, the troughs become increasingly small. However, as increasing amounts of rings are involved the total intensity of a trough's surrounding crest significantly de-

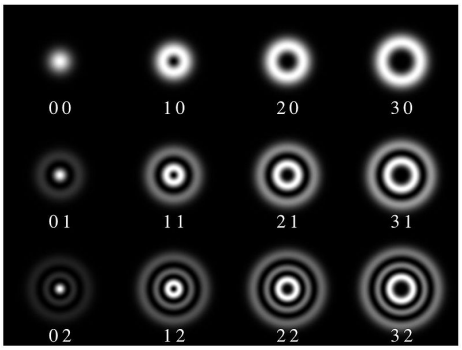

Figure 2: Intensity profiles of Laguerre Gaussian modes [8].

creases, damaging the effectiveness of the depletion spot.

Among the LG intensity modes, the LG_0^1 is the first to feature a trough. Because the diffraction pattern of an LG_0^1 beam is the simplest, it is a good candidate for a beam that is insusceptible to aberrations. Indeed, higher order LG modes show a less stable performance.

For these reasons, and because it is common practice within STED microscopy, I have chosen the LG_0^1 intensity mode as the main mode for the depletion spot. However alternative methods such as the $\lambda/2$ phase mask have also also been considered and used.

2.4 Aberration Correction

To re-adjust how the beam falls into the camera, aberration corrections are made such as 'tip', 'tilt' and 'defocus'. For this purpose I will use the Zernike modes, which are based on the Zernike correction terms. They can be theoretically understood as follows.

The wave front deformation

$$W(\rho,\theta) = \sum_{n=0}^{\infty}\sum_{m=0}^{n} z_{nm} N_n^m P_n^m \tag{2}$$

is described as the sum of specific Zernike wave front terms (or *modes*) Z_n^m. Each Zernike mode is described by the product of its Zernike orthonormal mode and a Zernike expansion coefficient. The orthogonal circle polynomial is given by

$$P_n^m(\rho,\phi) = \begin{cases} R_n^m(\rho)cos(m\phi) & \text{if } m \geq 0; \\ R_n^m(\rho)sin(m\phi) & \text{if } m < 0. \end{cases} \tag{3}$$

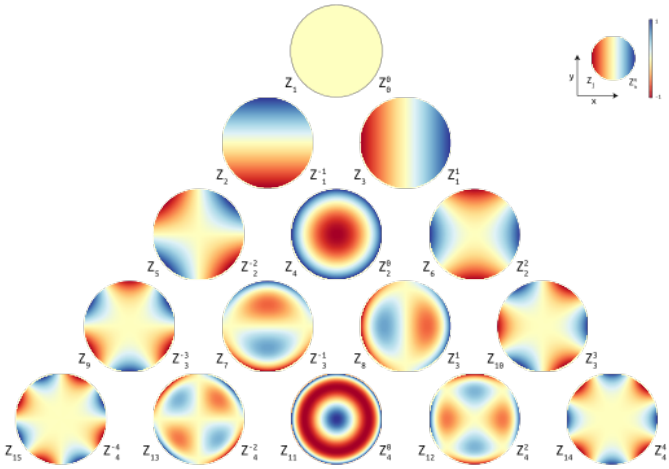

Figure 3: Zernike polynomial phase patterns [9].

Here the radial variable $R_n^m(\rho)$ is defined as

$$R_n^m(\rho) = \sum_{k=0}^{\frac{n-m}{2}} \frac{(-1)^k (n-k)!}{k!((n+m/2-k)!((n-m)/2-k)!} \rho^{n-2k} \tag{4}$$

The orthogonal polynomial is normalized by the factor $N_n^m = \sqrt{\frac{2(n+1)}{1+\delta_{m0}}}$.

The above equations generate a set of functions used to describe aberrations of optical systems. They represent the light phase patterns associated to these aberrations, as can be seen in Figure 3.

2.5 SLM

The Spatial Light Modulator, or SLM, comes from video projector technology but has found its way into research equipment. It is widely used for optical tweezers as well as for aberration corrections [2]. For the STED set-up, two LCOS-SLM's from Hamamatsu have been made available. These SLMs offer a grid of 792 by 600 squares, each square 20 µm in width. Light falls on each individual square, where it interacts with liquid crystals that are put under a voltage that can take can be set to 256 values, each allowing perturbation of the light's phase between 0 and a maximum of 2π.

I use the SLM to manipulate the generated Gaussian beam. Using mainly the LG_0^1 intensity modes and Zernike phase modes discussed in the previous section, the SLM allows the creation of phase patterns that generate the desired intensity patterns in that focal plane. Creating a LG_0^1 phase pattern allows a Gaussian beam to be masked by that pattern, so that when focused it forms

the LG_0^1 intensity mode.

Using an SLM for beam shaping imposes a trade-off between beam quality and beam complexity. The SLM's pixel array and discrete pixel values pose an upper limit on beam shape variety. As additional beam paths and aberrations are created, this limit becomes increasingly apparent through the deterioration of beam quality. I have invested a significant portion of the research in testing the limits to which the SLM can perform the desired functions. With the Hamamatsu SLM, at most 256 values are available for each pixel of the 792 x 600 array.

As desired phase masks become more complex, it is possible that the total resolution offered by the SLM becomes a limiting factor. In order to test if this is the case, experiments have been performed that try to simulate the levels of complexity that are desired.

2.6 Original Spot Shape

The depletion spot needs to be correctly generated by the Hamamatsu SLM, and appropriate software is needed for this. The Hamamatsu SLM comes with control software designed for the purpose of displaying phase masks. Its main function is to project a given phase mask onto the SLM monitor. To supply this software with the desired phase masks, supplemental code was available and was already being used with the STED microscope. It could generate the basic fork pattern. This pattern is formed by combining the LG_0^1 phase mask with the first Zernike phase mask; tilt. The combination is done by adding the two masks up before modulating the resulting phase mask to the modulo of 2π. Using the software in place allowed me to generate a phase mask with a resulting depletion spot that can be seen in Figure 4.

The spot with a trough in the middle is the depletion spot, while the lower dot is the beam that did not interact with the phase mask. The pattern at the top of the image is due to aberrations. The strange extra holes that seem to be surrounding the depletion spot are damaged parts of the camera. The spot generated with the software is of low quality due to a lot of the available intensity going into aberrations. To make the depletion spot suitable for STED, this needs to be addressed.

2.7 Phase Mask Ramp

Phase masks generated using third party code seemed to produce low quality depletion spots. The code used a sinusoidal ramp to generate the tip and tilt used in the fork pattern. The linear ramp provided by the Zernike equations was tried as an alternative for producing the tip and tilt, and the depletion beams produced by the two methods have been compared, the result of which

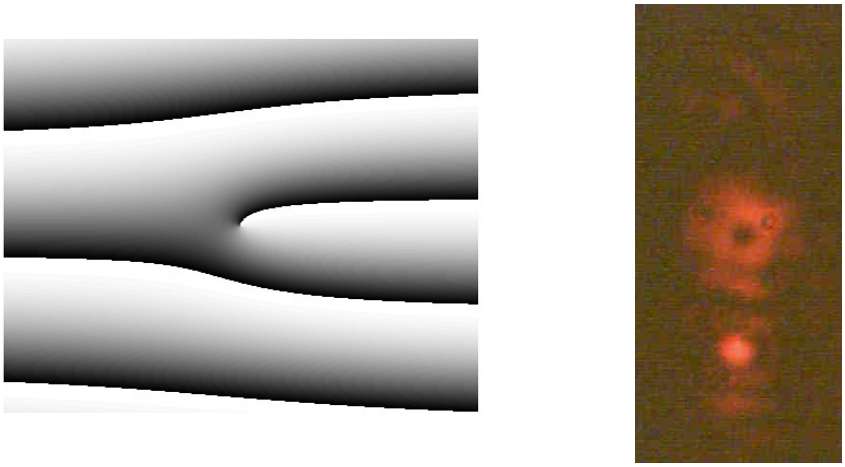

(a) fork pattern phase mask

(b) generated focal image

Figure 4: depletion spot generated by fork pattern

can be seen in Figure 5. The figure shows that the linear ramp produces results where the surrounding aberrations are reduced significantly. It suggests that the equations for the Zernike modes function better than the sinusoidal ramp found in the initial code. The sinusoidal ramp has therefore been abandoned and replaced by the linear ramp.

2.8 Multiple Depletion Spots

Besides STED, there is another often used fluorescence microscopy method known as Reversible Saturable Optical Fluorescence Transitions (RESOLFT). It differentiates itself from STED through the use of a different type of fluorophore which has to be activated first. Only when this has been done can they be deactivated. The benefit of RESOLFT compared to STED is that a much lower intensity is required for the lasers, drastically reducing the chance of fluorophore photo-bleaching. The downside is a longer fluorophore preparation time due to the mentioned difference. This is potentially destructive for microscopy purposes when a sample drifts away from its original position before a full picture can be taken where each confocal measurement is performed one after the other.

For the purpose of RESOLFT microscopy, it is useful to generate multiple depletion spots, as this allows fluorophores to be prepared simultaneously. To accommodate this, two main methods that split the SLM among the different spots have been tested and compared. They are here named the spatial split method and the phase split method.

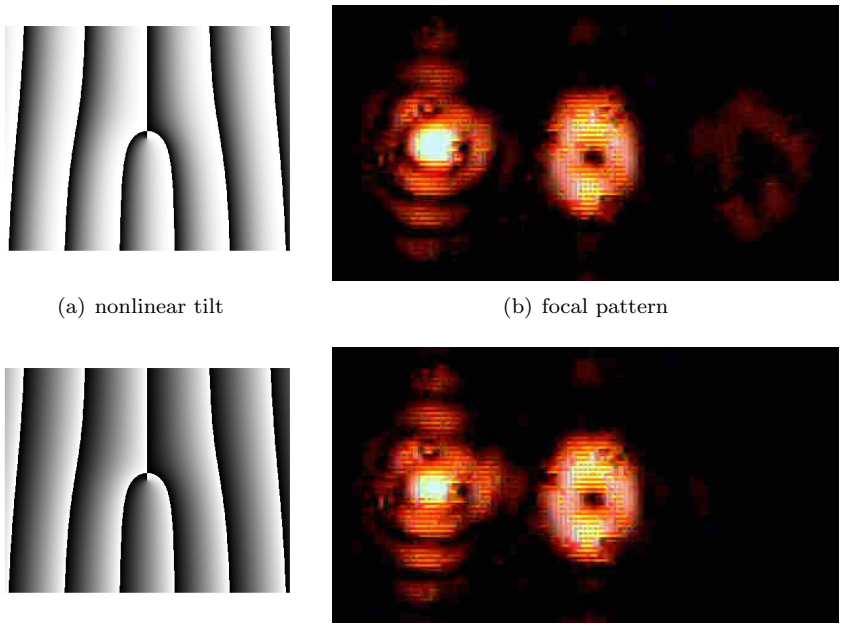

(a) nonlinear tilt (b) focal pattern

(c) linear tilt (d) focal pattern

Figure 5: Linear and non-linear tilt patterns

The spatial split method divides the SLM phase mask into separate windows, where each window is used to generate only one spot and a different window can generate different spots. The drawback here is that any spot generated this way has less surface of the phase mask available to it for its generation. The resulting lower numerical aperture of the spot will increase its width and consequentially decrease RESOLFT sharpness. In order to measure this, several phase masks, with each having an increasingly large surrounding frame, were generated carrying the same pattern. The effect of this can be seen in Figure 6.

The focal spots can be seen to become increasingly larger and darker as the phase pattern window becomes smaller. The donut shape, however, remains intact. This has also been confirmed for Figure 6 (h) by re-measuring it at higher laser intensity.

In order to measure the effect of spatially split phase patterns, the SLM window was divided into two, four and sixteen separate areas, as is shown in Figure 7. In this figure, it can be seen that the mask with two separate patterns produces two separate, distinct depletion patterns. However, the symmetry is also significantly affected. This can be explained by the inhomogeneous intensity distribution of light on the SLM. Each separate pattern now experiences

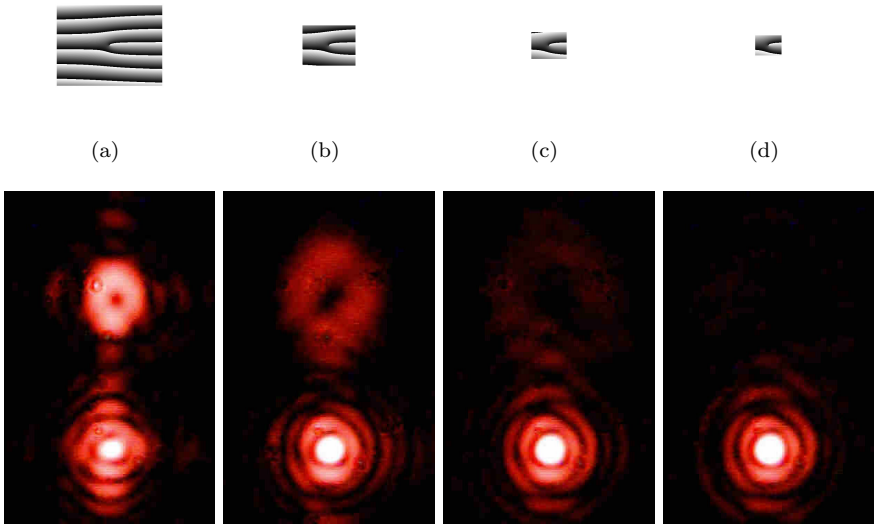

Figure 6: Phase masks with varying frame sizes together with their resulting focal spot.

not an illuminating Gaussian beam, but instead only a cut-off of that beam. A solution for this is to make the separate windows smaller and larger in number, allowing you to divide the patterns more evenly over the Gaussian beam shape.

The figures that carry the four and sixteen separate patterns show a problem. In the areas where the donuts used to be the resulting pattern becomes increasingly incomprehensible and immediately unfit for super-resolution microscopy. Aberrations have distorted the donut pattern. Causes for these patterns are the interfaces between all the windows, which increase in number as more separate windows are created. At these interfaces the phase masks conflict, causing significant aberrations. It has been confirmed that moving the four-pattern mask, so that the laser spot illuminates the upper two patters, gradually creates the pattern of Figure 7 (d).

The second method splits the SLM's range of phase modulation among the different spots. This means that each spot is generated using a phase mask whose phase modulation range is $2\pi/n_s$, where n_s is the amount of spots. This allows each spot to use the full surface of the phase mask, thus retaining a high NA. However, it also means that the phase cannot be shifted by an entire period. With this method, a phase mask therefore cannot have a continuous phase pattern over multiple periods. If this is required, there will be a discrete step where the mask goes back to 0 phase shift. I tested this method by overlapping

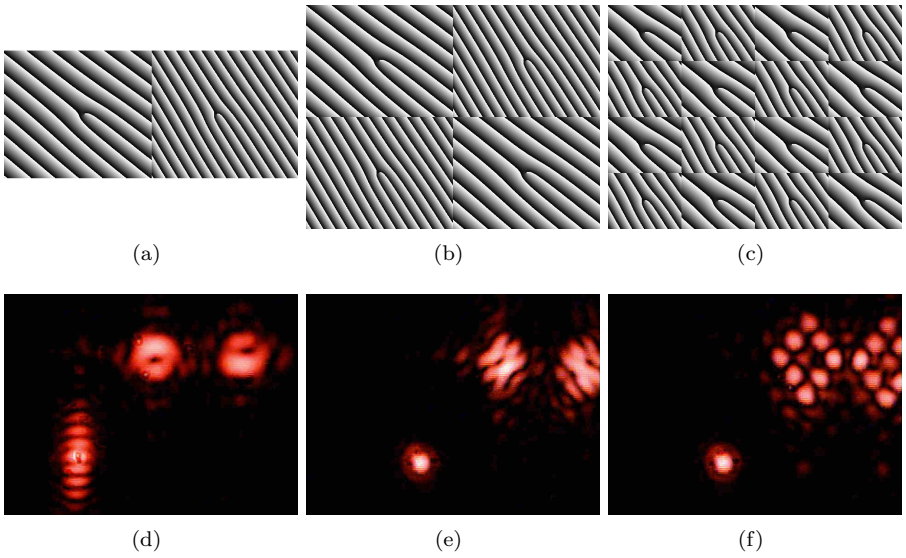

Figure 7: Spatially split phase masks together with their resulting focal spot.

multiple fork patterns. Each fork pattern on its own has a different tilt and would generate a focal spot on a different position. The results are shown in Figure 8.

The overlapping patterns perform remarkably well. The different donut patterns retain their shape as more are added, while overall intensity is evenly distributed among the individual patterns. They also assume the position that is expected when each pattern would be displayed individually. Furthermore, there is no sign of any significant aberrations as a result of the limited phase range that is available to each pattern.

2.9 Conclusion

The linear ramp of the tilt patterns, as well as the phase split method, yield very positive results when compared to their alternatives and have been used as the default methodology from here on out. However, during these measurements, problems were encountered in the effectiveness of the software.

To gain sufficient control over the SLM, a software tool had to be found that offers enough flexibility for prototyping methods within RESOLFT microscopy. The Hamamatsu SLM control software that comes bundled with the SLM proved itself too rigid for this purpose. It required any phase mask to be loaded from a file, after which very limited manipulations were possible,and would not serve the purpose of controlling complex patterns in later applications. A substitute

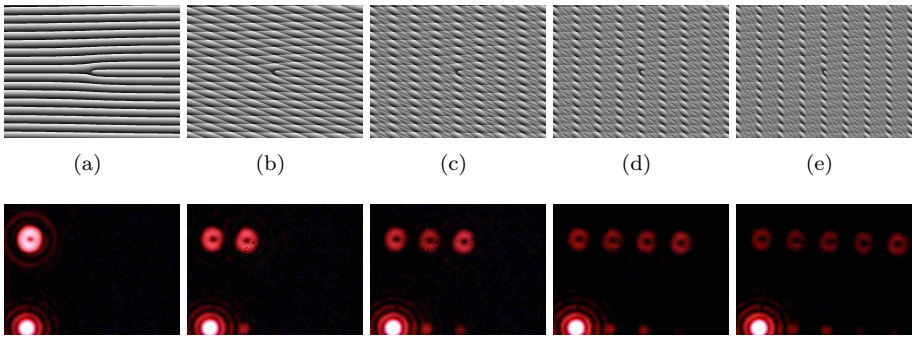

Figure 8: Phase split phase masks along with their resulting focal spot.

was needed.

Besides the way in which the software features were performed, it was also inconvenient for our purposes that the generation of the phase masks had to be done outside of the software. Calculating the phase masks away from the environment that controlled the SLM quickly became too time consuming when experimenting with different phase masks,

A new program has been built that directly projects generated phase masks to the SLM monitor. Further more, the ambition for this software is to incorporate it into the control software of the STED set-up. For this purpose, it has been built using the same platform as that of the set-up's main control software; LabVIEW. This platform is suitable both because it allows the separately created software to work together and because it allows for intuitive hardware control.

The new program was built on existing LabVIEW code used in Canada, which was provided by Gerhard Blab. This code originally performed functions such as generating the first twelve Zernike modes and projecting a phase mask onto the SLM. It has been made compatible with the Hamamatsu X10468 LCOS-SLM and converted to perform all the required features of the original Hamamatsu control software. From there on it has been further developed to allow intuitive control over features desired for RESOLFT microscopy.

The new control software was created alongside a set-up separate from the main STED set-up, which is treated in the following section.

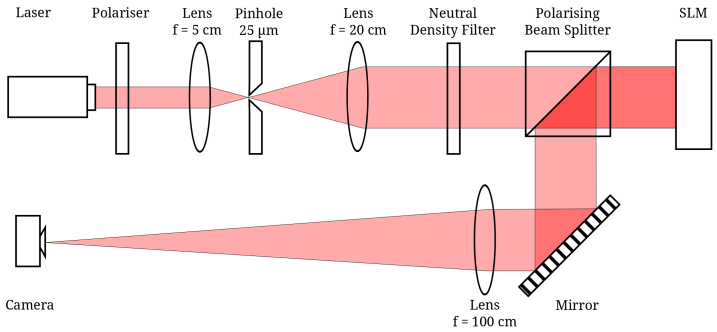

Figure 9: depletion set-up

3 Depletion Set-Up

In this section, the depletion set-up is introduced, which has been constructed to allow for more isolated experimentation on the SLM and the generated focal spot pattern. The experiments on depletion pattern creation, aberration correction and multiple beam generation are treated.

3.1 Introduction

The depletion set-up is a simplified segment of a functional STED microscope, focusing on depletion spot formation. It ideally projects a Gaussian beam onto an SLM and focuses the diffracted pattern on a camera and can be seen in Figure 9.

When the beam is generated using a polarized laser beam, it is not yet Gaussian. This is approximately corrected by applying a telescope with a 25 micrometer pinhole at the focus, creating an Airy disk. Because the beam's angle of incidence with respect to the SLM is zero a beam splitter cube is placed before the SLM, redirecting the refracted beam. A final lens focuses the beam into a depletion spot and a camera is placed in that focus to image the spot. Because the depletion spot can become too strong for the camera, a variable intensity filter is also placed before the beam splitter cube.

Further specifications of the set-up, such as the focal length of the final lens, the strength of the intensity filters and even the laser used are subject to change among the various experiments performed.

For the initial experiments done with the set-up, a Phoxx 642 nm continuous wave laser was used with a variable intensity output of up to 100 mW and a roughly 25 µm beam waist. Later, this laser was replaced by a 670 nm laser operating in the order of 1 mW.

An optimization routine for the optics positioning was used as follows. The laser is projected on a far field surface where a dot is then marked. Each optical element subsequently placed in the beam path is calibrated to center the beam on the marking. This routine applies to the polarizing filter, the telescope and the intensity filters.

After the first telescope lens is positioned, the pinhole is locked on the telescope focal point by gauging the total intensity emanating from the hole and maximizing this.

When the pinhole is calibrated, the second telescope lens is repositioned to ensure that the telescope produces a straight beam. This is done by measuring the beam width both at the exit point of the telescope and in the far field.

If the resulting beam width is not suitable for the desired experiment, the second telescope lens is replaced by a more appropriate substitute, which is then re-positioned following the same method described.

The SLM is initially calibrated by using the refracted pattern that moves back into the telescope. In the telescope focal plane, the beam will be focused on the pinhole surface. The SLM can be placed perpendicular to the beam path by positioning this focal spot inside the pinhole.

The polarizing splitter cube is placed before the SLM. While I do not use its polarizing properties, it does serve as a simple signal splitter. This reduces the total intensity as it transmits through the cube onto the SLM, and again as the beam diffracts off the SLM and is reflected 90 degrees by the cube.

The reflected beam is used for a second calibration of the SLM. Projecting the beam on a white surface, the frame of the SLM grid is seen to envelop the Airy disk. The SLM can now be positioned so the disk resides in the center of the frame. To facilitate this, a cross-hair phase mask has been created. It allows not only the frame to be visible, but also a circular pattern centered on the frame center. This makes adjusting the beam position significantly more convenient.

For the positioning of the focusing 1 meter lens, a marked spot is again used in the far field for reference. For different experiments requiring different numeric apertures, different lenses are used. The depletion spot is generated at the lens focus, where the camera is positioned to image the spot.

The resolution of the image at the focal plane can be estimated by using the par-axial wave approximation to determine the focal beam width

$$w_0 \approx \frac{4\lambda}{\pi\Theta} \tag{5}$$

of a Gaussian beam. Here λ is the wavelength of the laser light and Θ is the total angular spread of the focusing beam. For an image of diameter H passing through the focusing lens with focal length f we know that $\Theta = \tan^{-1}(H/f)$. This gives a focal plane magnification M_0 $(= 2w_0/H)$ of

$$M_0 \approx \frac{8\lambda}{\pi \tan^{-1}(H/f)H} \tag{6}$$

3.2 Basic Beam Shape

To assess the quality of the depletion spot I have defined four dimensionless quantities to construct a quality factor. They are *trough/crest intensity ratio*, *spot symmetry*, *spot size* and *spot sharpness*. To quantify these, the camera images are used with the background intensity subtracted; $I_(x, y) = I_{camera}(x, y) - I_{background}$.

The trough intensity I_{min} must be as low as possible while maintaining an average surrounding crest intensity I_{max} strong enough to de-activate surrounding fluorophores. This is expressed by the quantity I_{min}/I_{max}.

Spot size is determined by the size of the trough. This is attained from the fit by defining the radius $\vec{w_a}(\theta, r_a)$ and perpendicular radius $\vec{w_b}(\theta, r_b)$. The average radius is taken as $(|\vec{w_a}| + |\vec{w_b}|)/2$.

Spot symmetry uses the same vectors and is defined $|\vec{w_a}|/|\vec{w_b}|$.

To determine the depletion spot properties, a fit is performed that creates an intensity pattern which matches the image data of the spot. This fit should allow parameters to be varied in order to account for minor aberrational effects. A full analytical solution of the Laguerre Gaussian beam under the influence of aberrations is available [5]. However, this analysis is too time consuming to be used for any live, iterative process used within adaptive optics. Instead, the energy of the depletion beam at the focal plane is approximated by the following function;

$$E_f(r) = cr^b e^{-r^2}. \tag{7}$$

here c is an energy scaling factor. r is the par-axial distance from the spot center. The position of the spot center is defined as x_0,y_0. These values are found during fitting by defining $r = \sqrt{(x - x_0)^2 + (y - y_0)^2}$. b is a parameter that is included in order to allow the equation to adjust the bluntness of the trough. The sharpness of a donut van be quantified as $1/b$. The energy is used to determine the intensity pattern $I = |E_f|^2$. This intensity will always have

a zero intensity at the trough center. To account for any depletion spot image where this is not the case, a weak Gaussian profile is added to the intensity profile.

I have generated a depletion beam by applying a fork pattern phase mask. The beam has been imaged under optimal conditions and the above equation has been used to fit the beam. The result is shown in Figure 10.

The relative minimum trough intensity I_{min}/I_{max} is zero. This is due to the camera being unable to detect any light at all at the center of the spot. In order to detect as much of the trough intensity as possible, the laser intensity has been tuned so that the maximum intensity of the depletion beam approaches the maximum detectable level of the camera. However, even then the trough is too dark to pick up. The average radius of the donut beam is 137 μm, with a symmetry factor $|\vec{w_a}|/|\vec{w_b}| = 1.05$. The sharpness 1/b = 1.49.

It can be seen that the fitted curve slightly overestimates the higher intensity levels of the beam, and underestimate the lower values until the actual zero intensity point is reached. This is a general indication that the intensity pattern does not perfectly fit the assumed profile. This can be due to the camera being less sensitive at higher intensity levels, or because the beam provided to the SLM is not perfectly Gaussian. It is after all an Airy disk that has been cut off by the SLM window.

3.3 Aberrations

The depletion beam pattern is susceptible to aberrations both from the optical setup and the target sample. Common aberrations in a STED set-up are tip, tilt, defocus, coma and astigmatism [3]. The Zernike phase masks used to counter these distortions of the focal spot require characterization. Firstly because they themselves generate aberrations making them ideal for studying the effect of aberrations on the generated LG_0^1 beam. Secondly because any future adaptive optics scheme requires them to be functioning properly.

The tip and tilt have been applied to the depletion beam using varying Zernike phase modes and various angles of the mask perpendicular to the beam path. The Zernike phase mode of the tip and tilt are given simply by $Z_1^{-1} = zcos(\theta)$ and $Z_1^1 = zsin(\theta)$ respectively, where z is the Zernike coefficient used to increase the aberration strength. The minimum intensity of the depletion beam's trough as a function of the Zernike coefficient can be seen in Figure 11. The intensity values are discreet because they are the lowest intensity values which the camera is able to pick up. The tip and tilt aberrations respond linearly to the increase of the coefficient. This indicates that any unwanted aberrations are not interfering with the intended displacement.

Another negative effect that might occur is the effect of tip and tilt on the

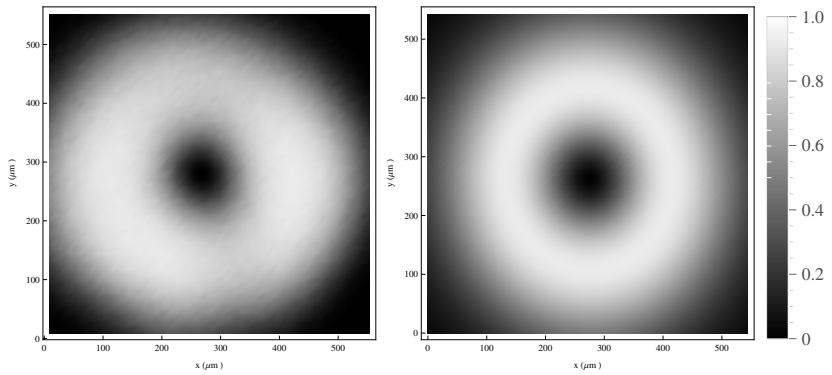

(a) depletion image (b) depletion fit

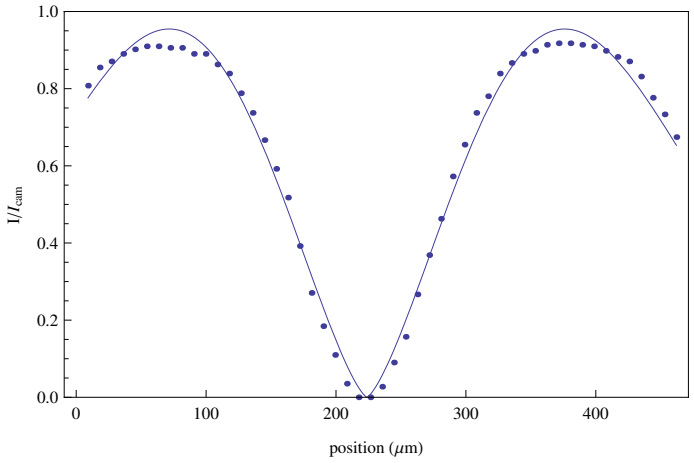

(d) cross section

Figure 10: Intensity pattern of a depletion beam image (a), its fitted function (b) and a cross section of the two (d), in values relative to the maximum camera intensity.

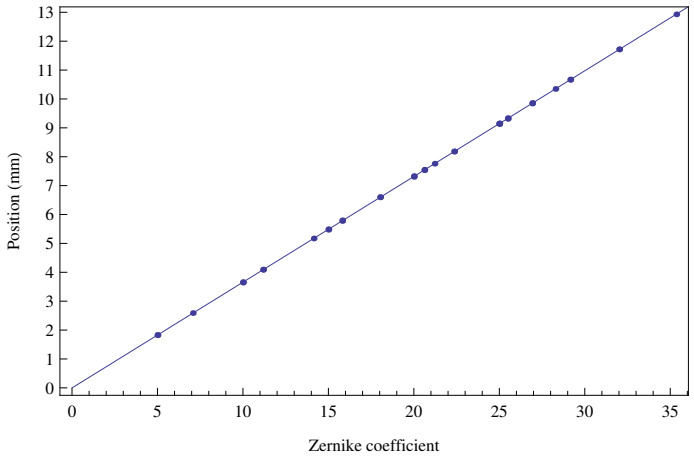

Figure 11: Trough position as a function of the tilt Zernike mode coefficient. 35 coefficients were used, some of which were of equal value but apply to varying tilt angles of the phase mask.

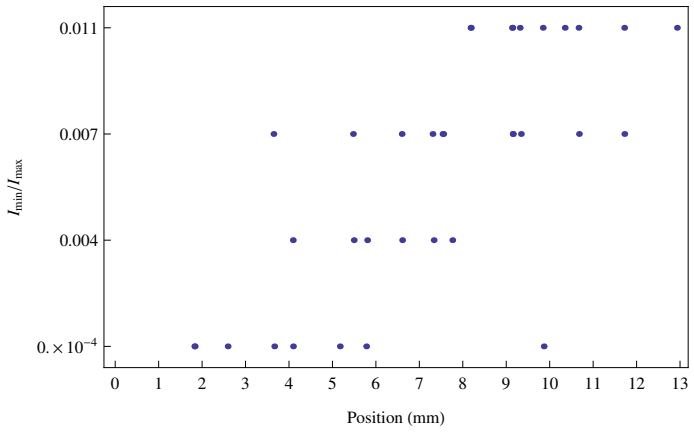

Figure 12: Trough minimum intensities I_{min} relative to the maximum intensity I_{max} of the initial trough as a function of spot position.

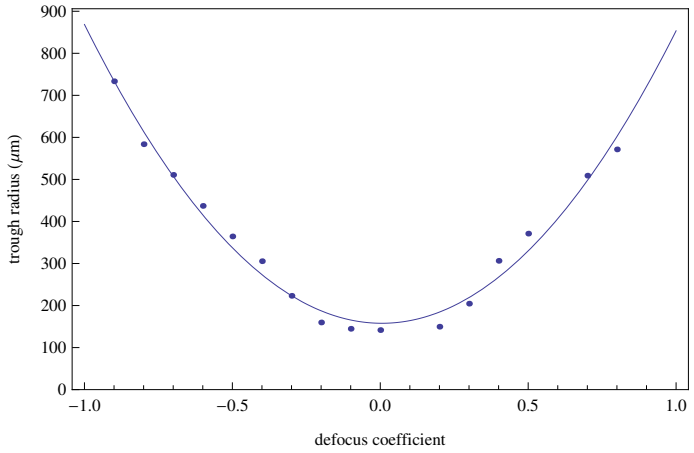

Figure 13: Spot width at several defocus values

minimum intensity of the depletion trough. This has been characterized in Figure 12. While the minimal intensity does seem to increase as the trough displacement increases, the data is too chaotic to discern any specific relation. A reason for this effect can be that the total variation between the trough minima is equal to the intensity change found when moving one pixel away from the minimum. This indicates that even at the 1 meter focal length of the focusing lens, the resolution is still a limiting factor in analyzing the trough minimum.

To further allow the usage of Zernike modes for aberration correction, the Zernike defocus mode has been characterized. The corresponding phase mask is defined as $Z_2^0 = z\sqrt{3}(2r^2 - 1)$ [6], where z is the Zernike coefficient. As usual, it has been combined with a tilt phase mask (with a tilt coefficient of 5) and the LG_0^1 helicoidal phase ramp. The known effect of the defocus mask on the donut beam is that the donut shape will grow larger and larger as the defocus increases. For this reason the distance between the trough minimum and crest maximum is taken from fits performed on donuts that were created using increasing Zernike defocus coefficients. The result of this can be seen in Figure 13.

The results are easily fitted to a quadratic polynomial of the form $ax^2 + b$. The resulting parameters are a = 716 ± 28 μm^{-1} and b = 137 ± 10 μm. Because this polynomial of the trough radius as a function of the Zernike defocus coefficient clearly has only one minimum, the trough radius is a simple value by which to optimize the defocus in an adaptive optics scheme.

The coma and astigmatism Zernike modes have also been implemented and produce behavior similar to that expected from simulation [3]. However, the fitting routine used is not suitable for characterizing these modes, as it cannot reproduce the asymmetry they create in the depletion spot. A suitable solution

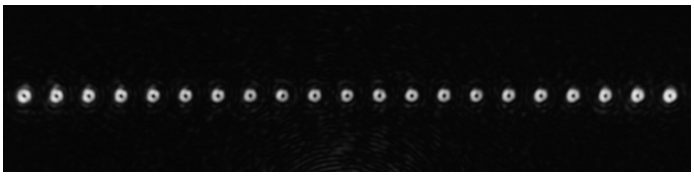

Figure 14: 21 spots with image dimensions of 11.25 mm by 2.71 mm.

for this within the context of fast computation still needs to be found.

3.4 Phase Split Method

The phase split method that has been previously discussed has been further studied within the current set-up. Key questions are the extent to which the minimum value of the trough minimum intensity and symmetry of the depletion spot are preserved when increasingly large amounts of depletion beams are being generated. Another question is what the spot behavior is like when being brought in close proximity to each other, and the extent to which they still remain functional.

Measurements have been taken where increasingly large amounts of donuts were generated using the phase split method, as can be seen from Figure 14.

For each donut that is added to the simultaneous generation, intensity will be taken away from the ones that were already there. Without the consideration of aberrations it would be reasonable to assume that the intensity of each individual donut would scale linearly with the total amount of donuts. To verify the scaling, the relative intensity of a donut was determined for an increasing amount of surrounding donuts. The results can be seen in Figure 15. As can be seen, a significant non-linear effect is present. This could in part be due to the non-linear method in which the donuts were placed. Because they all had to fit within the range of the camera, they were positioned on a 5 by 5 grid instead of a single line.

When two depletion spots are brought in close proximity they will gradually become less defined. The result of bringing two donuts increasingly close together is shown in Figure 16. The multiple spots gradually start interfering with each other more and more. The interference pattern of identical spots is seen to gradually become merged and unfit for use as separate depletion spots. At a separation of 535 µm, the spots still have a distinct own property whose bulks have 50% of their original power left. But from there on the depletion spot crests merge and the troughs are no longer isolated.

To circumvent the issue of canceling out phases, the LG_0^1 phase masks have

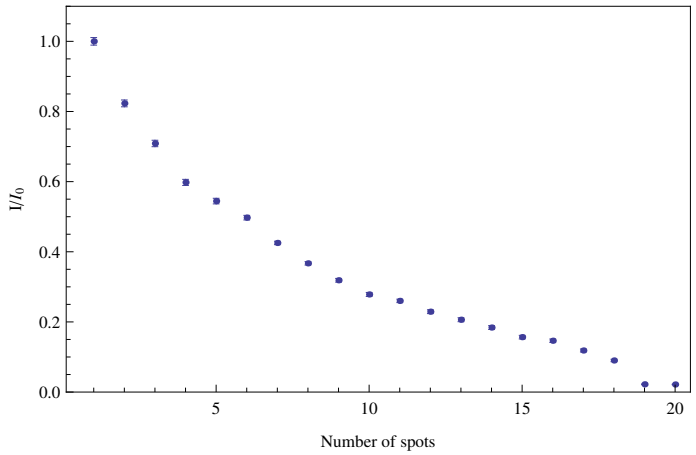

Figure 15: Spot intensity as a function of total spot amount, relative to the intensity for one spot.

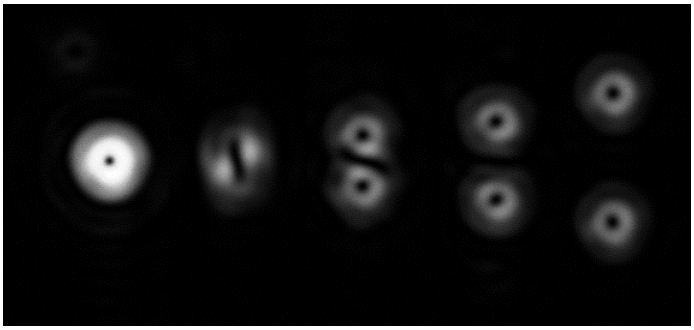

Figure 16: Composite image of two spots gradually being brought closer. The image dimensions are 7.28 mm by 3.40 mm.

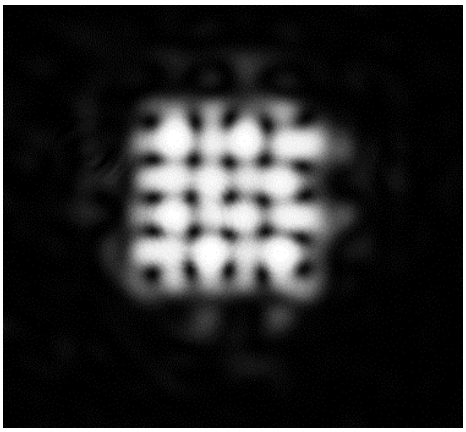

Figure 17: Grid of close packed spots using mirrored and rotated phase masks. The image dimensions are 3.40 mm by 3.13 mm.

been rotated and mirrored with respect to each other in order to create a constructively interfering interface between the generated spots. This can be done for only two spots, but the method can also be expanded to account for an array of spots positioned on a square grid. The best result of these attempts can be seen in Figure 17. As can be seen, the individual troughs are still very distinct even when being in very close proximity to each other. However, the pattern becomes very susceptible to aberrations and it becomes increasingly difficult to keep the pattern uniform.

Care should be exercised when using multiple spots in close proximity, as their interference can be destructive. However, the central software has been expanded to allow individual LG_0^1 phase masks to be mirrored and rotated, allowing spots to be brought closer to each other. This process is still limited by uniformity destroying aberrations that increase as spots are brought closer together.

3.5 Polarization

The Hamamatsu SLM is designed to modulate the phase pattern while leaving both the intensity pattern and the polarization pattern unperturbed. However, even when this is the case, the focusing lens combined with the phase pattern could cause unwanted changes in the polarization pattern. Such an effect would have considerable influence on polarization sensitive fluorophores.

The set-up has been designed to make it possible to both polarize and measure the depletion spot in the focus, by stretching the beam focus long enough for both the camera and the polarizing plate to be within the focal area. This is

done by the lens of one meter focal length. Rotating the polarizing plate around the direction of the beam path in steps of 20° produces Figure 18.

As can be seen, the polarization falls within the behavior expected from a uniformly polarized beam, suggesting that the polarization is unchanged within the spot focus. However, it remains to be said that the far field approach of this measurement might not account for the behavior of a spot generated by a high NA lens. Also, some differing aberrations can be seen among the measurements at different angles. This can be explained by the structural integrity of the polarizing plate. Indeed when the plate was perturbed, the aberrations where seen to move along with it.

To verify the expected intensity shift that accompanies the shifting polarization filter, a sine wave was fitted to the maximum intensity of the beams, as can be seen in Figure 19.

3.6 Phase Mask Symmetry

The symmetry of the depletion spot can be very easily broken by positioning the airy disk away from the SLM's center. It can be seen that when the Airy disk is moved away from the center of the SLM, significant effects occur in the focal spot. Most notable, the trough of the depletion spot starts to move away from the spot's center, gradually approaching and destroying the spot's crest. To address this I incorporated a function within the SLM software that allows the phase mask pattern to be displaced along the SLM window. The effect of the moving trough center disappears when you reposition the phase mask so that it is nicely aligned with the displaced Airy disk again. This process has greatly improved the quality of the depletion beam. Especially in the longer direction of the SLM (792 pixels), it is much more efficient to readjust the SLM phase mask than to perfectly align the laser. However, not all aberration effects are mitigated in this fashion.

Even when the phase mask is re positioned to correct for a positioning shift of the Airy disk, the beam can still be asymmetric. While the trough is now nicely in the center of the surrounding crest, they can lose their circular shape and even their ellipsoidal shape as the Airy disk is positioned further away from the SLM's center. A possible and likely cause for this, is that the boundary of the SLM phase mask isn't point symmetric. Even when a phase mask pattern is shifted to let the center coincide with the Airy disk center, the beam leaving the SLM will not be symmetric due to the phase mask's rectangular boundaries. As was previously shown in Figure 6, smaller phase masks generate larger depletion spots. The question therefore arose whether an asymmetric phase mask would cause significant asymmetry in the depletion spot.

To test this, a new phase mask modification was made, where the mask is cut off by a circular frame. Light falling on this frame will not experience a

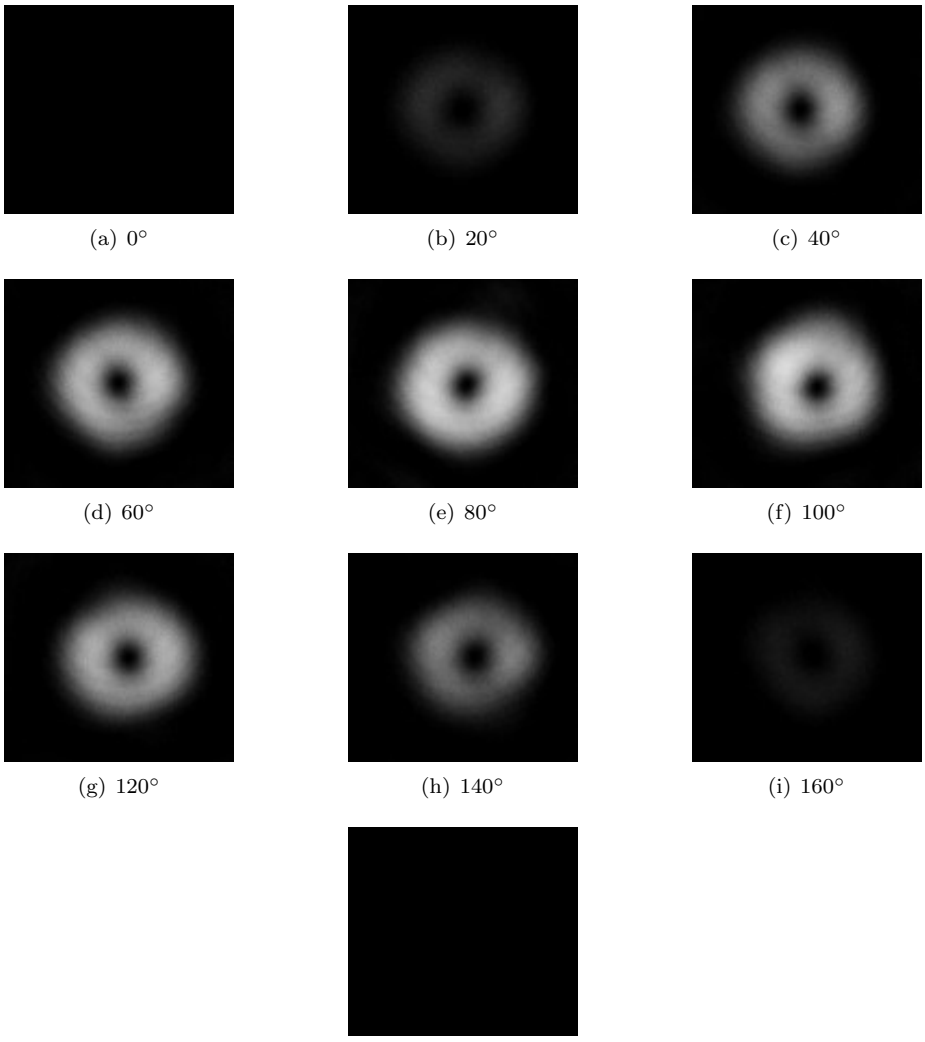

(a) 0° (b) 20° (c) 40°

(d) 60° (e) 80° (f) 100°

(g) 120° (h) 140° (i) 160°

(j) 180°

Figure 18: Polarization measurement of depletion spot. The image dimensions are 960 µm by 870 µm.

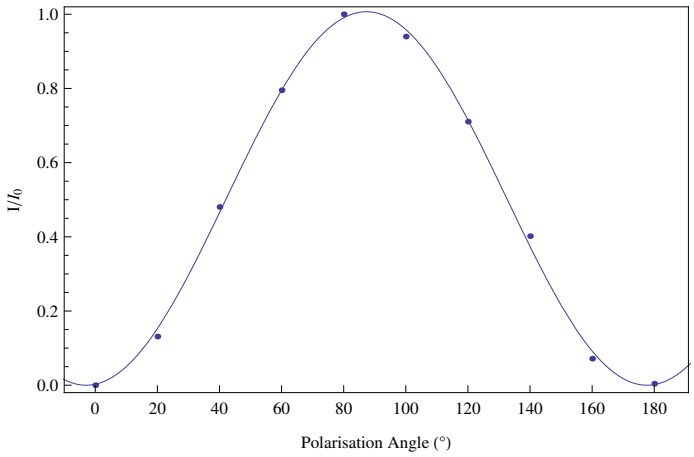

Figure 19: depletion spot intensity relative to the highest intensity, as a function of polarisation angle.

phase shift from the SLM. Therefore if both the phase mask pattern and circular frame are centered around the airy disk center, no asymmetry should be left in the SLM system. The results of these measurements can be seen in Figure 20.

3.7 $\lambda/2$ Phase Mask

An alternate phase mask used to generate the donut pattern is the $\lambda/2$ mask, which shifts the phase of the mask's inner circle by half a phase in order to create destructive interference at the circle interface. This interference performs the same function as the vortex center of the LG_0^1 phase mask. A Z-stack of this image is shown in Figure 21.

The results show a depletion spot that has a very clear intensity lobes on the optical axis, both before and after the focal plane. The lobes set the $\lambda/2$ spot apart from the LG_0^1 spot which does not show any intensity anywhere on the optical axis. This is as expected, as the $\lambda/2$ beam is often used for 3D imaging where this resolution is required. However, the trough waist shows itself to be significantly smaller than that of the LG_0^1 phase mask. As our STED set-up is intended for the study of thin samples, this property has precedence over the z-resolution, however for added flexibility the $\lambda/2$ phase mask is included to allow the study of deeper samples.

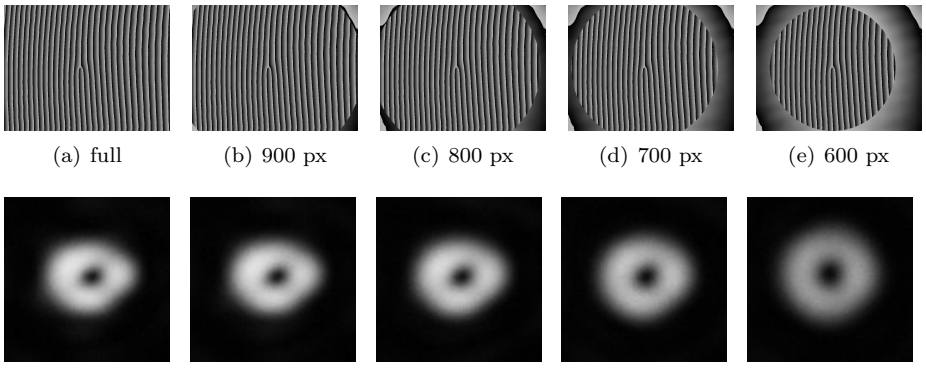

(a) full (b) 900 px (c) 800 px (d) 700 px (e) 600 px

(f) full (g) 900 px (h) 800 px (i) 700 px (j) 600 px

Figure 20: focal spots (f)-(j) of phase masks (a)-(e) with increasingly small frame diameter (given in each caption). The camera image dimensions are 906 µm by 906 µm.

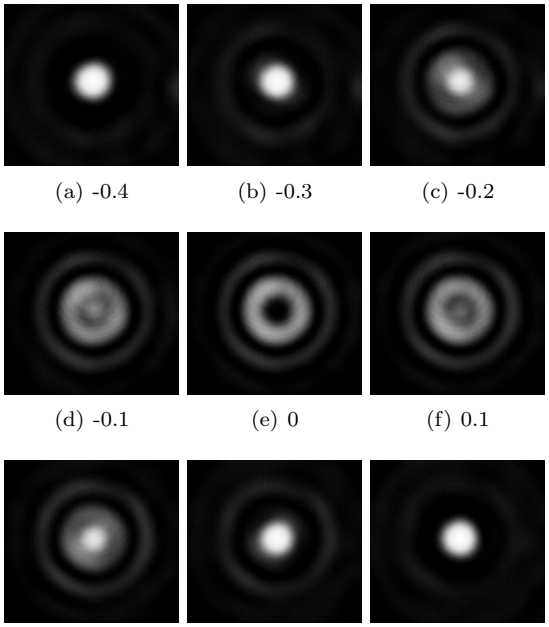

(a) -0.4 (b) -0.3 (c) -0.2

(d) -0.1 (e) 0 (f) 0.1

(g) 0.2 (h) 0.3 (i) 0.4

Figure 21: Z-stack of the $\lambda/2$ depletion spot, along with the corresponding Zernike mode parameter. Image dimensions are 1.60 mm by 1.50 mm.

4 Conclusion

In this section the research is concluded, summarizing the attained results, discussing problems that have occurred and projecting possible courses for future research.

4.1 Results

The Spatial Light modulator has been used to generate a depletion beam suitable for STED microscopy. A basic depletion beam has been generated using the helicoidal phase ramp that generates a Laguerre Guassian beam, and the method of generation has been optimized. It has been shown that with full illumination of a camera with the ability to pick up a scale of 256 different light values, the depletion beam can be generated with a central intensity too weak to be picked up by the camera. This is the best indication of a zero intensity center the set-up could create.

Zernike modes have been implemented with a twofold function; the ability to further engineer the basic pattern of the depletion spot and the ability to correct for aberrations along the way. The performance of the Zernike modes corresponding to the aberrations most common in a STED set-up; tip, tilt, defocus, coma and astigmatism, has been tested. The tip and tilt a very linear relation between the applied Zernike coefficient and the depletion spot displacement. The defocus shows that the beam waist as a function of the Zernike coefficient is described very well by a second order polynomial. Coma and astigmatism have also been implemented and tested, and show good correspondence to literature.

For the purpose of using the Zernike modes for the correction of aberrations in an adaptive optics set-up, a fitting routine has been created and tested. It uses an equation that can be fitted very rapidly and is able to generate quantities that can tell an adaptive optics scheme the tip, tilt and defocus coefficients should be made larger or smaller. The routine does not however provide the same function for coma and astigmatism.

Methods have been explored for the generation of multiple donuts. While the spatial split method seems too sensitive to aberrations, the phase split method has produced very good results. The intensity of each individual donut does vary when creating several, but tools have been created to balance the intensity out. However, the problem of relative trough minimum intensity being different per donut still remains. The changing of phase orientation of each spot's phase mask has been used in an attempt to pack spots more closely together, and it has been shown that indeed spots can be in a much closer proximity to each other before the troughs start becoming indistinguishable. However, this again occurs at the expense of the minimum trough value and spot symmetry.

In closing, the SLM can adequately perform such functions as are required for adaptive optics within RESOLFT microscopy. Creating a depletion spot by combining a singularity mask with aberration masks is fully feasible within this context, and a method has been tested that allows aberrations to be tested at a speed sufficient for a feedback loop, although coma and astigmatism still require a more time consuming fitting routine.

4.2 Discussion

The results for adaptive optics have not yet been applied to a microscopy set-up. It would require joining three aspects that so far have remained separate; the camera, the SLM control software and the code used to analyze the camera images. While many compatibility issues have already been addressed for the current set-up, some might still arise, such as between the outdated NIKON camera and the LabVIEW software used for the SLM control.

However, before more time is invested into the current set-up, it must be mentioned that it has been suggested [6] that adaptive optics is best performed with a sample image instead of a depletion beam image. This has been treated in the research of Tim van Werkhoven [7]. The possibility of automating this with an SLM might very well be more profitable than pursuing an adaptive optics set-up with the current set-up that focuses on the focal plane image of the depletion spot.

Regardless, the irregularities observed when multiple depletion spots are produced suggest that the SLM is not the ideal device for this specific purpose. It has been shown in this research that there are methods of managing the coherence among multiple depletion spots, such as individually tuning the spot intensity and adapting the phase ramp orientation, however these complications might be avoided altogether by exploring alternatives, as is suggested by recent research [1].

While it wasn't in the scope of this research, there is an interest in exploring the possibilities of the Gerchberg-Saxton algorithm, which allows custom patterns to be generated. While its iterative approach might not be ideal for manufacturing a basic depletion pattern, it could be very suitable for compensating more complex aberrations and could be used as an addition to the current fitting routine.

Another point concerning my research is that when fitting to the intensity profiles taken with the NIKON camera, often the fitted function rose above data points that where within the upper twenty percent of intensity that the camera could register. It suggests that perhaps the NIKON camera is less sensitive to light in this upper area.

The laser used for the STED microscope has been replaced after I did my research. Originally the a 643 nm activation and 780 nm depletion beam were produced. This has been dropped roughly by 150 nm. The microscope now produces a 405 nm activation beam and a 532 depletion beam. These wavelengths are not effective for the ATTO 647N but work well with ATTO 425 which is used as the replacement fluorophore.

4.3 Thanks

I'd like to thank Hans Gerritsen for accepting and starting my guidance in this group, Gerhard Blab for continuing this guidance and for the never ending supply of Austrian chocolates and Imaad Mohammed for always being there to help and to talk with. I'd also like to thank Dave van der Heuvel for keeping everything running smoothly including the coffee breaks, and all the members of the biophysics group for the great time I've had there.

5 References

References

[1] J. Keller et al. A. Chmyrov. Nanoscopy with more than 100,000 doughnuts. *Nature Methods*, 10(8):737–742, August 2013.

[2] S. Bernet C. Maurer, A. Jesacher and M. Ritsch-Marte. What spatial light modulators can do for optical microscopy. *Laser Photonics*, 5(1):81–101, 2011.

[3] J. Bai et al. C. Zhang, K.Wang. Simulation studying effects of multiple primary abberations on donut-shaped gaussian beam. *Optics and Photonics*, 3:1–5, 2013.

[4] S.W. Hell and J. Wichmann. Breaking the diffraction resolution limit by stimulated emission: stimulated-emission-depletion fluorescence microscopy. *Optics Letters*, 19(11):780–782, June 1994.

[5] P. Senthilkumaran R.K. Singh and K. Singh. Effect of primary spherical aberration on high-numerical-aperture focusing of a laguerregaussian beam. *Optical Society of America*, 25(6):1306–1318, January 2008.

[6] D. Burke et al. T.J. Gould. Adaptive optics enables 3d sted microscopy in aberrating specimens. *Optics Express*, 20(19), August 2012.

[7] T. van Werkhoven. *Lasers, lenses and light curves*. PhD thesis, Leiden University, 2014.

[8] Wikipedia. `"http://en.wikipedia.org/wiki/Gaussian_beam#mediaviewer/File:LG-wiki.jpg"`.

[9] Wikipedia. `"http://en.wikipedia.org/wiki/Zernike_polynomials#mediaviewer/File:ZernikePolynome6.svg"`.

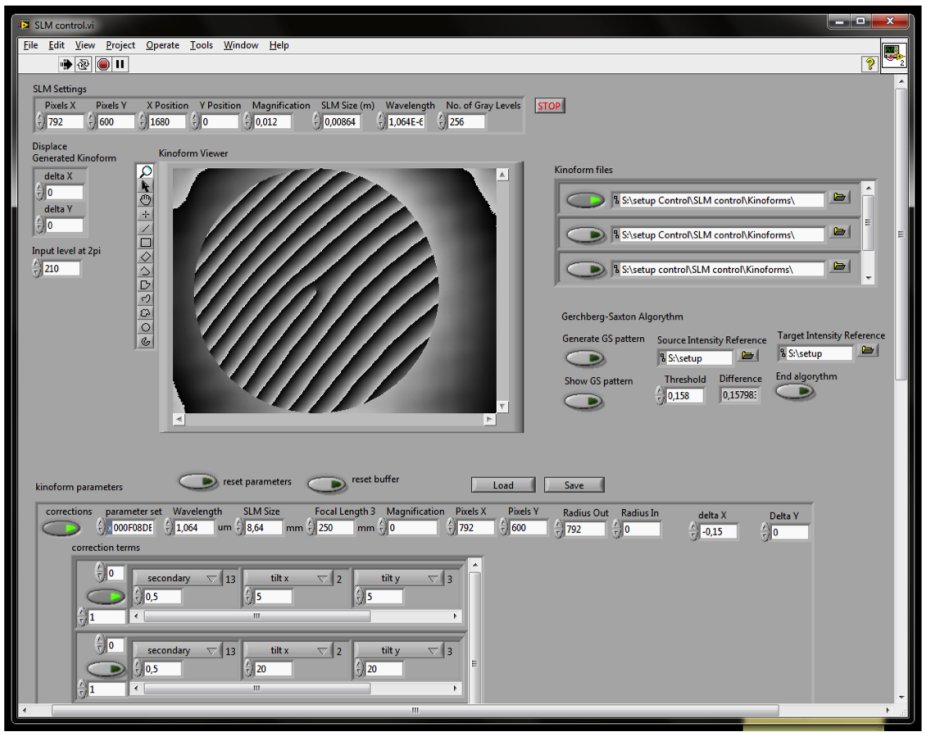

Figure 22: SLM control software

6 Appendix

In this section the software used for generating the phase masks is described and its features are listed.

The main function of the developed software tool is to 'instantly' generate phase mask patterns relevant to STED microscopy, in a way that is compatible with the software already in place for the built STED set-up. The latter is done by building the program within LabVIEW, which is the platform in which all other set-up control modules have been written. Seeing this software tool as just another module seemed like the most natural choice and has been the design philosophy for the tool.

The module is controlled through a single interface, an example of which can be seen in Figure 22. Each interface area is titled, so they should be easy to reference to. The most prominent one is the Kinoform Viewer. 'Kinoform' as a term was used analogously to 'phase mask' during the creation of the software tool, but was abandoned at the time of writing this thesis. It shows the array that is being projected on a secondary monitor which can be picked up by the

SLM. The gray values range from white to black, representing an integer value from 0 to 256. When this value is read out by the SLM, it applies a corresponding voltage to the elements of its liquid crystal array, and depending on the wavelength of the light beam, a certain phase shift is induced.

Stark contrast from whites to blacks can be seen because the phase mask is modulated so that a light beam will be subjected to a phase shift of no more than one whole phase. The SLM includes a datasheet unique to that model, indicating what array integer value creates an entire phase shift for specific wavelengths. This is the value we want to use for the modulation and it can be entered in the input field left of the kinoform viewer titled 'input level at 2pi'. The image shows an input of 210, meaning that the phase mask uses a range of 210 grey values.

Above the Kinoform Viewer is the SLM Settings area. This is important for telling the software how big the SLM is which you intend to used (through 'Pixels X' and 'Pixels Y') and where you want the total phase mask to be projected as a second monitor ('X position' and 'Y position'. For example, in Figure 22 these values are 1680 and 0, placing the second monitor right next to a primary screen that's 1680 pixels wide, and positioning it at the same height. The software is run on the Windows 7 operating system, which then allows you to define the position of a second monitor to overlap with the given specifications.

To the right of the viewer if the kinoform files section. This allows you to directly load phase masks from a stored file and display them. The SLM comes with correction phase masks for specific wavelengths, so it is advised to load this mask before continuing. Images are stacked by adding the arrays and modulating the whole after the addition. Phase masks can be stored through the right-click menu of the Kinoform Viewer.

The area used to generate the Laguerre Gaussian phase masks and the Zernike phase masks is 'Kinoform Parameters'. The 'correction' button allows this section to be switched on or off. Whenever changes are made, it is advised that you press 'reset parameters' right above this area. The input fields to the right of the corrections button perform various functions. The fields 'parameter set' through to Magnification' are legacy, and at the moment do not have a proper function. Pixels X and Pixels Y define the pixel dimensions of the SLM. Radius out determines the radius of a circular window within which the LG and Zernike phase masks are generated. This circle can be seen in Figure 22. Setting the Radius Out to 0 places the radius at infinity. The circle can also be given an inner radius through the Radius In input field. This ensures that the phase masks will not be generated within this radius. The parameters Delta X and Delta Y allow the window to be positioned along the Kinoform Viewer, taking the generated phase masks along with it. This is an important tool used to center the mask around the lightbeam, as discussed in section 3.6.

The phase mask patterns are created in the 'correction terms' area within the 'kinoform parameters' area. Each row is a separate phase masks. These masks are combined using the phase split method described in Section 2.8. Each row contains a button which switches this row on or off and an input field to give a weight to the phase mask generated in this row, as discussed in section 3.4. Each column of a row allows you to select a mode type. The Zernike modes are named, with a total of twelve Zernike modes being available. The thirteenth option is the LG_1^0 mask and the fourteenth option is the $\lambda/2$ mask. The input field below the mode selection is the Zernike coefficient when a Zernike mode is selected, the angle of the mask when the LG_1^0 is selected (for purposes mentioned in Section 3.4), and a radius when the $\lambda/2$ mask is selected. The masks of all columns in a row are added before they are modulated, generating hybrid patterns such as the fork pattern. Any configuration of the kinoform parameters area can be saved and loaded with the two respective bottoms right on top of the area.

There are some more input fields and buttons which are not treated here. Most of them are experimental (i.e. they do not have a functional purpose yet), but can be traced back to their function through the LabVIEW interface. Most notable among these is the Gerchberg-Saxton Algorythm area, to the right of the Kinoform Viewer. This section was intended to create patterns generated by the Gerchberg-Saxton algorythm, which at some point became a side track in the research project. However, this was never completed and has not yet generated a functional phase mask.